THE JOURNAL OF BIOLOGICAL CHEMISTRY VOL. 287, NO. 49, pp. 41258–41267, November 30, 2012

Heterogeneity of ATP-sensitive K^+ Channels in Cardiac Myocytes

ENRICHMENT AT THE INTERCALATED DISK[*S]

Received for publication, August 20, 2012, and in revised form, October 10, 2012 Published, JBC Papers in Press, October 12, 2012, DOI 10.1074/jbc.M112.412122

Miyoun Hong[‡1], Li Bao[‡1], Eirini Kefaloyianni[‡], Esperanza Agullo-Pascual[§], Halina Chkourko[§], Monique Foster[‡], Eylem Taskin[‡], Marine Zhandre[‡], Dylan A. Reid[¶], Eli Rothenberg[¶], Mario Delmar[§], and William A. Coetzee[‡¶‖2]

From the Departments of [‡]Pediatrics, [§]Medicine, [‖]Physiology & Neuroscience, and [¶]Biochemistry and Molecular Pharmacology, New York University School of Medicine, New York, New York 10016

Background: K_{ATP} channels are abundantly expressed in cardiac myocytes.
Results: K_{ATP} channels interact with desmosomal proteins and localize to the intercalated disk.
Conclusion: K_{ATP} channels are heterogeneously expressed within a cardiac myocyte.
Significance: K_{ATP} channels may have role at the intercellular junctions during cardiac ischemia.

Ventricular ATP-sensitive potassium (K_{ATP}) channels link intracellular energy metabolism to membrane excitability and contractility. Our recent proteomics experiments identified plakoglobin and plakophilin-2 (PKP2) as putative K_{ATP} channel-associated proteins. We investigated whether the association of K_{ATP} channel subunits with junctional proteins translates to heterogeneous subcellular distribution within a cardiac myocyte. Co-immunoprecipitation experiments confirmed physical interaction between K_{ATP} channels and PKP2 and plakoglobin in rat heart. Immunolocalization experiments demonstrated that K_{ATP} channel subunits (Kir6.2 and SUR2A) are expressed at a higher density at the intercalated disk in mouse and rat hearts, where they co-localized with PKP2 and plakoglobin. Super-resolution microscopy demonstrate that K_{ATP} channels are clustered within nanometer distances from junctional proteins. The local K_{ATP} channel density, recorded in excised inside-out patches, was larger at the cell end when compared with local currents recorded from the cell center. The K_{ATP} channel unitary conductance, block by MgATP and activation by MgADP, did not differ between these two locations. Whole cell K_{ATP} channel current density (activated by metabolic inhibition) was ~40% smaller in myocytes from mice haploinsufficient for PKP2. Experiments with excised patches demonstrated that the regional heterogeneity of K_{ATP} channels was absent in the PKP2 deficient mice, but the K_{ATP} channel unitary conductance and nucleotide sensitivities remained unaltered. Our data demonstrate heterogeneity of K_{ATP} channel distribution within a cardiac myocyte. The higher K_{ATP} channel density at the intercalated disk implies a possible role at the intercellular junctions during cardiac ischemia.

The cardiac myocyte is a highly polarized cell. The end to end connection between cardiomyocytes, called the intercalated disk (ICD),[3] includes three distinct junctional complexes: adherens junctions, desmosomes, and gap junctions, as well as a "mixed" structure dubbed the area composite (1). Junctional proteins, which are concentrated at the ICD, are responsible for integrating structural information and communication between myocytes. Desmosomes and adherens junctions are best known for their role in mediating mechanical coupling between cells, but there is a growing appreciation for the integrated nature of junctional complexes and for how aberrant cell-cell coupling, mediated through any of these junctional complexes, leads to cardiomyopathies and arrhythmia risk. For example, mutations in desmosomal proteins are linked to the heart muscle disorder known as arrhythmogenic cardiomyopathy (AC), characterized by fibrofatty infiltration, sustained ventricular tachycardia, and sudden cardiac death (2). Almost half of the AC patients carry a mutation in one of the five genes encoding desmosomal proteins expressed in the heart. Mice deficient of plakoglobin (PG) recapitulate many features of AC (2). At first sight, it is difficult to visualize the functional relationship between a structural element (the desmosome) and electrical events (arrhythmias). Recent data have helped to clarify the picture with the demonstration that some ion channels, such as the Na^+ channel and some K^+ channels (including Kv1.5 and Kir2.1), are enriched at the ICD (3–5). Moreover, there is growing evidence for interaction between desmosomal proteins and certain ion channels and that disruption of the desmosomal complex affects the function of these channels (4, 6, 7).

The role of ATP-sensitive K^+ (K_{ATP}) channel in metabolo-electrical coupling, defined as the relationship between intracellular energy metabolism and membrane excitability, is well described. Decreases in cellular ATP levels and elevated levels of ADP and AMP increase their open probability with resulting

* This work was supported, in whole or in part, by National Institutes of Health Grants HL105046 (to L. B.); R01-HL085820 and R21-HL093563 (to W. A. C.); and R01-HL106632 and P01-HL087226. This work was also supported by a grant from the Leducq Foundation (to M. D.).
[S] This article contains supplemental text and Figs. S1 and S2.
[1] These authors contributed equally to this work.
[2] To whom correspondence should be addressed: NYU School of Medicine, Alexandria Center for Life Science, 450 East 29th St., Floor 8 (824), New York, NY 10016. Tel.: 646-501-4510; Fax: 212-263-5100; E-mail: william.coetzee@nyu.edu.

[3] The abbreviations used are: ICD, intercalated disk; PG, plakoglobin; PKP, plakophilin-2; AC, arrhythmogenic cardiomyopathy; DP, desmoplakin; STORM, stochastic optical reconstruction microscopy; dSTORM, direct STORM; DNP, dinitrophenol; AnkG, ankyrin G.

physiological consequences that include the regulation of insulin release from pancreatic β-cells, vasodilation, changes in neuronal excitability, and control of neurotransmitter release. Sarcolemmal K_{ATP} channels consist of pore-forming Kir6 subunits, which obligatory assemble with regulatory SUR subunits (8). The Kir6 subunits (Kir6.1 and Kir6.2) determine the biophysical properties and nucleotide sensitivities of K_{ATP} channels. The SUR subunits (SUR1 and the two SUR2 splice variants, *e.g.*, SUR2A and SUR2B) fine-tune the nucleotide sensitivity and confer unique pharmacological specificities (8). Although the cardiac K_{ATP} channel has long been considered to be composed of Kir6.2/SUR2A combination, recent data demonstrate cardiac diversity, for example with a role for SUR1 in the atrium (9) and SUR2B in the specialized cardiac conduction system (10). A physiological role recently assigned to K_{ATP} channels in heart muscle is to regulate the action potential duration adaptation in response to elevated heart rates during exercise (11). A protective role of K_{ATP} channels against stress is also well documented (12, 13). A common implicit assumption is that sarcolemmal K_{ATP} channels are uniformly and statically expressed on the surface of cardiac myocytes. Our data, presented here, demonstrate nonuniform expression of K_{ATP} channels in cardiomyocytes with a pool of K_{ATP} channels enriched at the ICD of cardiac myocytes.

EXPERIMENTAL PROCEDURES

Animals—The investigation conformed to the U.S. National Institutes of Health Guide for the Care and Use of Laboratory Animals. Animal procedures were approved by the New York University Institutional Animal Care and Use Committee. We used adult male Sprague-Dawley rats (250–300 g; Charles River, Wilmington, MA), PKP2 (+/−) deficient mice (male, 4–5 months old) and their wild-type littermates (6). Ventricular myocytes were isolated enzymatically as described previously (14).

Membrane Preparations, Co-immunoprecipitation Assays, and Immunoblotting—Membrane fractions from cardiomyocytes were prepared, and co-immunoprecipitation experiments were performed using a previously described method (14).

Immunostaining—Immunohistochemistry was performed using methods adapted from previously described protocols (14, 15). Rat heart cryosections (6 μm) were dried, washed with PBS, and post-fixed in 4% paraformaldehyde for 10 min. Following permeabilization with a blocking solution (20% serum and 0.1% Triton X-100 in PBS) for 30 min, primary antibodies were applied 1–2 h at room temperature. After washing with PBS, secondary antibodies and DAPI were applied. Coverslips were mounted, and images were obtained using a laser scanning confocal microscope. Images were analyzed using ImageJ, which was also used to calculate Manders' co-localization coefficients (with Costes' automatic thresholding) using the JACoP plugin (16).

Super-resolution Microscopy—A modified staining protocol was used, optimized based on direct-STROM where the imaging buffer is supplemented with a reducing agent to promote blinking (17). Myocytes were first permeabilized with 1% Triton X-100 in PBS for 10 min and blocked for 30 min with solution containing 2% glycine, 2% BSA, 0.2% gelatin, and 50 mM NH_4Cl in PBS. Primary and secondary antibodies, conjugated to Alexa fluorophores, were diluted in the blocking solution and incubated for overnight at 4 °C and for 1 h at room temperature, respectively. Super-resolution imaging was done using a custom-built fluorescence microscope (Leica DMI3000) configured for total internal fluorescence and highly inclined excitation modes. Super-resolved images were constructed at 10 nm/pixel using the QuickPALM ImageJ plugin (18) and a mapping procedure written in IDL (Exelis Visual Information Solutions).

Antibodies Used—We used the following antibodies against K_{ATP} channel subunits: rabbit anti-Kir6.2 (Lee62; obtained from Dr. Hon-chi Lee, Mayo Clinic, MN), rabbit anti-Kir6.2 (W62b), chicken anti-Kir6.2 (C62(14)), goat anti-SUR2A (M-19, Santa Cruz), mouse anti-SUR2A (N319A, clone 14, Neuromab), and rabbit or chicken anti-SUR1 (RSUR1 or CSUR1). Antibodies used against desmosomal proteins included rabbit polyclonal anti-plakophilin-2 (ab74671; Abcam), mouse monoclonal anti-plakophilin-2 (K44262M; Life Science, Inc.), mouse monoclonal anti-plakoglobin (610254, BD Biosciences), mouse anti-N-cadherin (610920; BD Transduction Laboratories), mouse anti-ankyrin G (N106/36; NeuroMab), mouse anti-desmoplakin, rabbit anti-connexin43 (C6219; Sigma), rabbit anti-Kir2.1 (Alomone), rabbit anti-Kv4.2 (Sigma), and mouse anti-GAPDH (MAB374; Millipore). Secondary antibodies used were donkey anti-mouse-HRP (sc-2096; Santa Cruz Biotechnology), donkey anti-goat HRP (sc-2056; Santa Cruz Biotechnology), and goat anti-rabbit-HRP (sc-2054; Santa Cruz Biotechnology).

Whole Cell and Single Channel Recordings—Patch clamp recordings were performed as described before (10, 19). Whole cell current was recorded at a holding potential of −45 mV. Current-voltage relationships were obtained using a ramp protocol (5 mV to −100 mV at −25 mV·s^{-1}, applied every 20 s). Recordings were not corrected for the liquid junction potential, calculated to be −5 mV. For isolated patches, pipettes (1.5–3 MΩ) when filled with pipette solution: 150 mmol/liter KCl, 2 mmol/liter $CaCl_2$, 1.2 mmol/liter $MgCl_2$, and 10 mmol/liter HEPES, pH 7.4. The bath solution consisted of 150 mmol/liter KCl, 1 mmol/liter EGTA, 10 mmol/liter HEPES, and 1.2 mmol/liter $MgCl_2$, pH 7.2. Unless otherwise indicated, the pipette potential was +80 mV (membrane potential of −80 mV). Inward currents are represented as upward deflections in all figures.

Semiquantitative RT-PCR Analysis—Total RNA was extracted and reverse transcribed using a mixture of random hexamer primers, and semi-quantitative real time PCR was performed.

Statistical Analysis—All of the data are shown as the means ± S.E. (*n* denoting the number of cells), and differences between groups were determined using appropriate tests as specified in the text (SigmaStat; Systat Software Inc.), using a *p* value of < 0.05. Please see Supplemental text for expanded Experimental Procedures.

RESULTS

K_{ATP} Channel Subunits Associate with Plakoglobin and Plakophilin-2—In a recent proteomics screen, we identified glycolytic enzymes to be well represented in immunoprecipi-

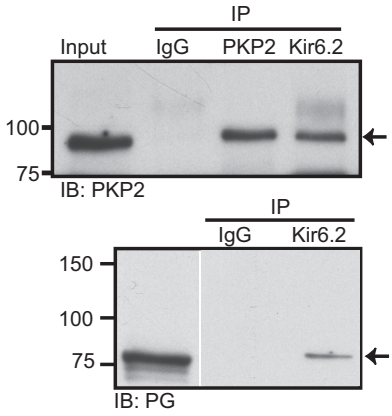

FIGURE 1. **Co-immunoprecipitation of K_{ATP} channel subunits and desmosomal proteins in rat heart.** *Top panel*, immunoprecipitates obtained with antibodies against Kir6.2 and PKP2 (IgG was used as a negative control) were subjected to SDS-PAGE and immunoblotted with a rabbit anti-PKP-2 antibody (1:200). *Bottom panel*, rat heart membrane immunoprecipitates obtained with IgG or rabbit anti-Kir6.2 (W62b) antibodies were immunoblotted with anti-PG antibodies. The specific bands are indicated by *arrows* and were not present in negative control reactions obtained with IgG. *IP*, immunoprecipitation; *IB*, immunoblot.

tates obtained with antibodies against K_{ATP} channel subunits (14). We also identified proteins that may provide hints to the localization and targeting of K_{ATP} channels, including the junctional protein PG and proteins that function in protein subcellular localization/stabilization and trafficking (including β-actin, tubulin, ARP-1, spectrin, and molecular motors such as dynein and myosins). In similar experiments (not shown), we also identified other proteins of the desmosomal complex, including desmoplakin (DP), desmoglein, and plakophilin-2 (PKP2). We verified interactions between PKP2 and PG with independent co-immunoprecipitation assays (Fig. 1).

K_{ATP} Channel Subunits Localize to Intercalated Disk Regions—We previously described the distribution patterns of K_{ATP} channel subunits in rat heart and ventricular myocytes. For Kir6.2, we described a sarcomeric striated pattern in ventricular myocytes. Closer inspection of our published images (15, 20), however, hints at the possibility of stronger staining at the intercalated disk regions. We therefore repeated this experiment by optimizing the staining/fixation conditions (*e.g.*, post-fixation was found to provide more robust tissue staining) and using newer well characterized antibodies (for example using an anti-Kir6.2 antibody from Dr. Hon-chi Lee). Kir6.2 staining was evident not only in cell membranes and striations across the cells, but additionally concentrated at the end to end junctions between cardiac myocytes (the ICD; Fig. 2*A*). We obtained similar data with other antibodies, including another anti-Kir6.2 antibody (C62) and a commercial antibody against SUR2A. Notably, both of these antibodies stained the ICD (evident in the overlay image). Other antibodies against K_{ATP} channel subunits also preferentially stained the cardiac intercalated disk, including a new monoclonal antibody against SUR2A (N319A, clone 14, NeuroMab; Fig. 2*C*), which specifically recognizes SUR2A (see specificity data on the Neuromab web site). Increased staining of Kir6.2 at cell ends was also observed in enzymatically isolated rat ventricular myocytes (Fig. 2*D*). With prolonged times after cell isolation (6–18 h), the cell ends became rounded, which was associated with a loss of localization of K_{ATP} channel subunits and ICD proteins (such as PG) at the cell ends (supplemental Fig. S1).

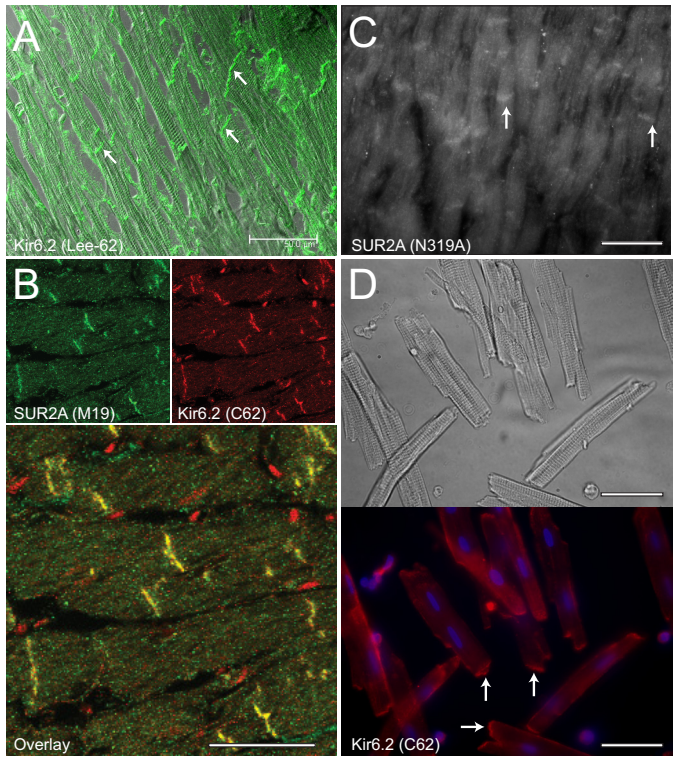

FIGURE 2. **Immunolocalization of Kir6. 2 and SUR2A at the ICD in rat hearts and isolated ventricular myocytes.** *A*, localization of Kir6.2 using a rabbit anti-Kir6.2 antibody (Lee-62; 1:300). *B*, co-staining with a commercial goat anti-SUR2A antibody (M19; 1:50; *green*) and with a chicken anti-Kir6.2 antibody (C62; 1:50). The overlay (*bottom panel*) depicts co-localization as *yellow*. The Manders' coefficients are M1 = 0.99 and M2 = 0.98. *C*, the result of an immunohistochemistry experiment of a rat heart cryosection when using a monoclonal anti-SUR2A antibody. *D*, bright field image and immunocytochemistry performed using isolated rat ventricular myocytes with the chicken anti-Kir6.2 antibody (C62; 1:50). The *arrows* indicate higher levels of staining at the ICD. The *scale bars* represent 50 μm.

K_{ATP} Channel Subunits Co-localize with Desmosomal Proteins—We next investigated the co-localization of K_{ATP} channels and desmosomal proteins. As expected, antibodies against PKP2 or PG strongly stained the intercalated regions of cardiac myocytes (Fig. 3). The subcellular expression of Kir6.2 was more diffuse but was enriched in the cell ends. Moreover, Kir6.2 staining overlapped with those of PKP2 and PG. Overlapping expression of desmosomal proteins with Kir6.2 and SUR2A was also observed in enzymatically isolated rat ventricular myocytes (not shown). Consistent with the intercalated disk localization of Kir2.1 (3), we also found this subunit to co-localize with PG, whereas Kv4.2 did not (supplemental Fig. S2).

The optical resolution of conventional microscopes is ~200 nm, and proteins that co-localize appear to overlay. Fluorescence images produced by stochastic optical reconstruction microscopy (STORM) allows superior subcellular localization of proteins and visualization of interacting proteins as adjacent particles at nanometer resolution (21). Direct STORM (dSTORM) (22) relies on the reversible photoswitching of fluorophores. A range of conventional dyes can be utilized with a "switching buffer" that causes cycling between the "on" and

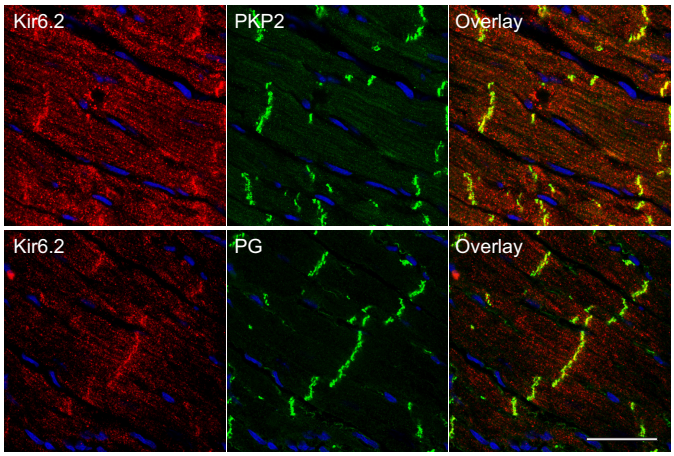

FIGURE 3. **K_{ATP} channel subunits co-localize with desmosomal proteins at the ICD.** *Top panels*, co-staining of a rat heart cryosection with the chicken anti-Kir6.2 antibody (C62; 1:50; *red*) and an antibody against PKP2 (1:200; *green*). *Bottom panels*, co-staining of a rat heart cryosection with the chicken anti-Kir6.2 antibody (C62; 1:50; *red*) and an antibody against PG (1:300; *green*). The panels on the *right* show the overlay of the *green* and *red*. The Manders' co-localization coefficients (using Costes' automatic thresholding) respectively are M1 = 0.882 and M2 = 0.996 (*top panels*) and M1 = 0.717 and M2 = 0.448 (*bottom panels*). The *scale bar* represents 50 μm.

"off" states (22) and allows an image to be constructed molecule by molecule, at a resolution approaching that of immuno-EM microscopy. We examined Kir6.2 and PKP2 localization at the ICD of an adult cardiac myocyte using total internal fluorescence microscopy, which improves the signal to noise ratio by rejecting out of focus fluorescence, and with dSTORM (Fig. 4). These images demonstrate clustered K_{ATP} channels in nanometer proximity of junctional proteins at the ICD.

Co-localization with Other ICD Proteins—We investigated whether K_{ATP} channels also co-localize with other proteins of the ICD. Cryosections of rat hearts were co-stained with antibodies against Kir6.2 and N-cadherin, which resulted in strong co-localization at discrete puncta at the ICD between cells (Fig. 5). As previously reported (23), AnkG staining was observed at the periphery of the cardiac myocyte, with stronger staining at the ICD. Kir6.2 also co-localized with AnkG at the ICD. Co-staining of AnkG and N-cadherin was also observed with antibodies against SUR2A (not shown). Co-localization was also observed between Kir6.2 and desmoplakin and to a lesser extent with Cx43. These data suggest the possibility of discrete structures enriched in K_{ATP} channels, possibly anchored by scaffolding proteins.

K_{ATP} Channel Current Density—We next performed patch clamp experiments to investigate the possibility that the K_{ATP} channel current would be higher when recorded from the cell ends. Measurements were made in the inside-out patch clamp configuration to record local current densities. The pipette was either placed near the center of isolated mouse ventricular myocytes or as close as possible toward the cell end (ICD region). Following patch excision, the current was recorded at −80 mV in the absence of ATP. Measurements were made immediately after patch excision to avoid run-down. Although there was a large variation in the mean patch current from patch to patch, the normalized open-state portability of KATP channel (NPo) was significantly larger when recorded from intercalated disk region (Fig. 6*A*). The averaged mean patch current was 769 ± 108 pA (n = 68, median 455 pA) when recorded from intercalated disk region compared with 414 ± 68 pA (n = 63, median 246pA) in patches obtained near the cell center. The difference in the median values between the two groups was greater than would be expected by chance ($p <$ 0.001, Mann-Whitney Rank Sum test). The pipette capacitances were similar between the two groups (1.4 ± 0.03 MΩ, n = 68 and 1.3 ± 0.02 MΩ, n = 63, respectively, for patches obtained near the center or ends of myocytes). In separate experiments, we also recorded K_{ATP} channel currents using the cell-attached patch clamp configuration before and after metabolic inhibition. A similar trend was observed, and currents recorded at the cell ends tended to be larger than those recorded near the cell center (Fig. 6*E*).

K_{ATP} Channel Properties—We examined the biophysical and regulatory properties of K_{ATP} channels using patch clamping in the inside-out configuration. The relationship between the unitary current and voltage was weakly inward-rectifying, and there were no differences between channels recorded near the cell center or ends (Fig. 6*B*). When recorded from the cell center, the K_{ATP} channel unitary conductance was 77 ± 2.6 pS (n = 5) compared with 75 ± 1.4 pS (n = 10) for channels recorded from the cell ends.

We also determined the sensitivity of K_{ATP} channels to intracellular nucleotides. A concentration-response curve for ATP inhibition was constructed by exposing patches sequentially to ATP between 3 and 3000 μM (Fig. 6*C*). There was no difference in the concentrations of ATP producing half-maximal inhibition (IC_{50}) when comparing patches obtained from the cell center and the intercalated disk regions (the median IC_{50} value was ~14 μM in each case; Table 1). We also examined the effects of intracellular MgADP on K_{ATP} channel activity. For these experiments, channels were partially inhibited by ATP (50 μM). ADP was then applied at an ADP:ATP ratio of 0.1–10 (Fig. 6*D*).Ventricular K_{ATP} channels were stimulated by lower MgADP concentrations but inhibited because the ADP concentration was high. There was no difference in the ADP sensitivity when comparing patches obtained from the cell center and the intercalated disk regions.

K_{ATP} Channels in the PKP2 Knock-out Mouse—Given the physical interaction of K_{ATP} channel subunits with desmosomal proteins such as PG and PKP2, we investigated the possibility that K_{ATP} channel currents may be affected when reducing expression of desmosomal proteins. For these experiments we employed heterozygous PKP2 knock-out animals (PKP2 ± mice) (24), in which PKP2 protein level in the heart is halved (6). Enzymatically isolated ventricular myocytes from the PKP2 (+/−) mice were subjected to whole cell patch clamping, and K_{ATP} channel current was activated following application of dinitrophenol (DNP; 100 μM). The current-voltage relationships of the DNP-activated currents are shown in Fig. 7*A*. The K_{ATP} channel current density was significantly smaller in the PKP (±) myocytes. For example, at −10 mV the maximal current in the presence of DNP was 149 ± 17.3 pA/pF (n = 14) in wild-type myocytes compared with 91 ± 11.2 pA/pF (n = 17; $p < 0.05$ Student's t test) in PKP2 (+/−) myocytes.

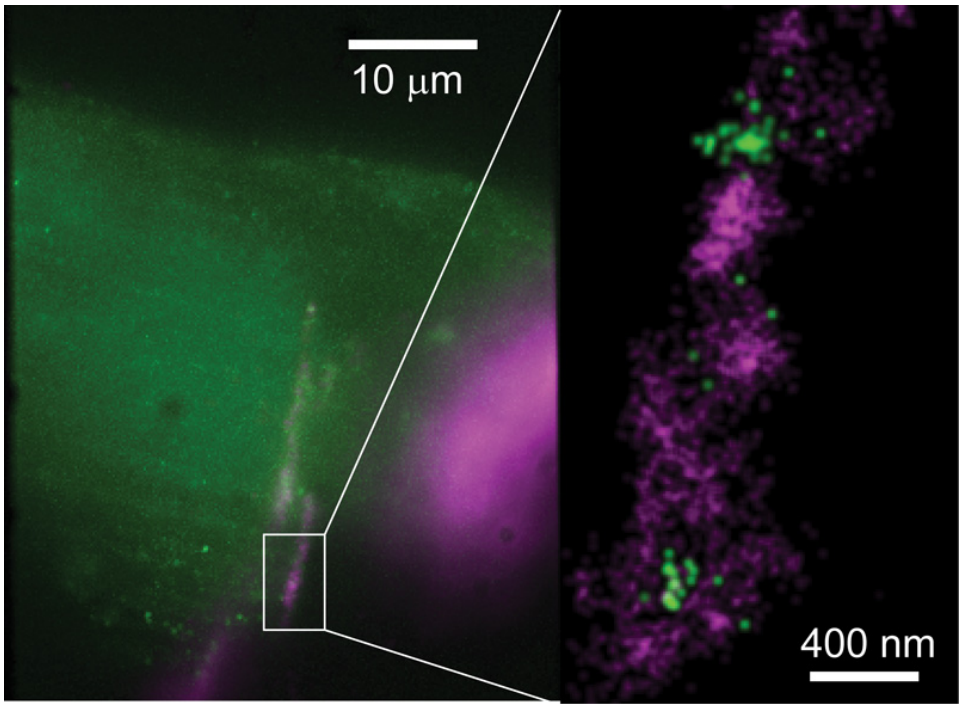

FIGURE 4. **Nanometer resolution determination of K_{ATP} channel localization at the ICD of an enzymatically isolated rat ventricular myocyte.** *Left panel*, total internal fluorescence microscopy of Kir6.2 (*green*) and PKP2 (*magenta*) of the ICD. At this resolution, co-localization appears as *white* when using this color model. *Right panel*, dSTORM microscopy of the *boxed area*, demonstrating that K_{ATP} channels are juxtapositioned within nanometer distances from PKP2.

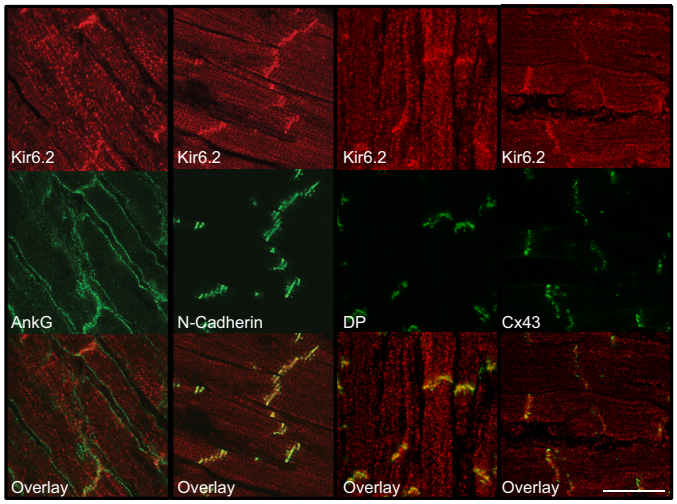

FIGURE 5. **Co-localization of Kir6. 2 with proteins of the ICD.** Co-staining was performed (from *left* to *right*) with Kir6.2 and AnkG (1:50), N-cadherin (BD Transduction Laboratories; 1:500), DP (1:200), or connexin 43 (Cx43; Sigma; C6219, 1:1000). Kir6.2 was staining was with Lee62 (1:300) in all *top panels*, except for the *third column* where C62 (1:50) was used. The *scale bar* is 50 μm.

We next investigated K_{ATP} channel properties in excised patches from ventricular myocytes of PKP2 (+/−) mice. The unitary conductance was not different when comparing patches obtained from the cell centers with those from the intercalated disk regions (Table 1). Moreover, there was no difference in unitary conductance when comparing data from wild type with data from PKP2 (+/−) mice. We also investigated the mean patch current. In the wild-type mouse, the mean patch current was significantly larger in patches excised from the cell end compared with patches obtained from the cell center (Table 1 and Fig. 7*B*). In contrast, this difference was not observed in myocytes from the PKP2 (+/−) mouse. In patches obtained from the cell ends, the mean patch current was ~30% smaller in the PKP2 (+/−) mice, which closely matches the decreased whole cell current density. In patches obtained from the cell center, ATP inhibited the K_{ATP} channel of PKP (+/−) myocytes with an IC_{50} value indistinguishable from wild type (Table 1). In contrast, ATP sensitivity of K_{ATP} channels from cell ends in the PKP2 (+/−) myocytes was right-shifted when comparing with the cell center or with wild-type data (Table 1 and Fig. 7*C*). There was no apparent difference in MgADP sensitivities of K_{ATP} channels in PKP2 (+/−) myocytes, regardless of their localization (Fig. 7*D*). There were no differences in the mRNA expression of the K_{ATP} channel subunits (Kir6.1, Kir6.2, SUR1, total SUR2, or SUR2A) or protein expression of Kir6.2 or SUR2A between the hearts of wild-type and PKP2 (+/−) mice (Fig. 7*F*). Using biochemical techniques, we estimated that ~70% of the total K_{ATP} channel subunits are localized in intracellular (endosomal) compartments (19), and the unchanged protein levels are therefore not expected to equate the reduced whole cell current density (Fig. 7*G*).

In immunohistochemistry experiments of mouse heart cryosections, we found that that K_{ATP} channel subunits were still localized at the ICD in the PKP2 (+/−) mice (N-cadherin was used as an ICD marker; Fig. 7*E*). We calculated the Manders' co-localization coefficients (with Costes' automatic thresholding) of the immunohistochemistry data, which shows that 6.4 ± 0.75% ($n = 6$) of the total Kir6.2 signal overlaps with that of N-cadherin in WT mouse heart cryosections, which contrasts with 3.8 ± 0.16% ($n = 6$; $p = 008$ Student t test) in the PKP2 (+/−) mouse heart. It should be noted that the confocal images were taken through the cell interior, suggesting that a component of Kir6.2 staining may be intracellular, supportive of our previously pub-

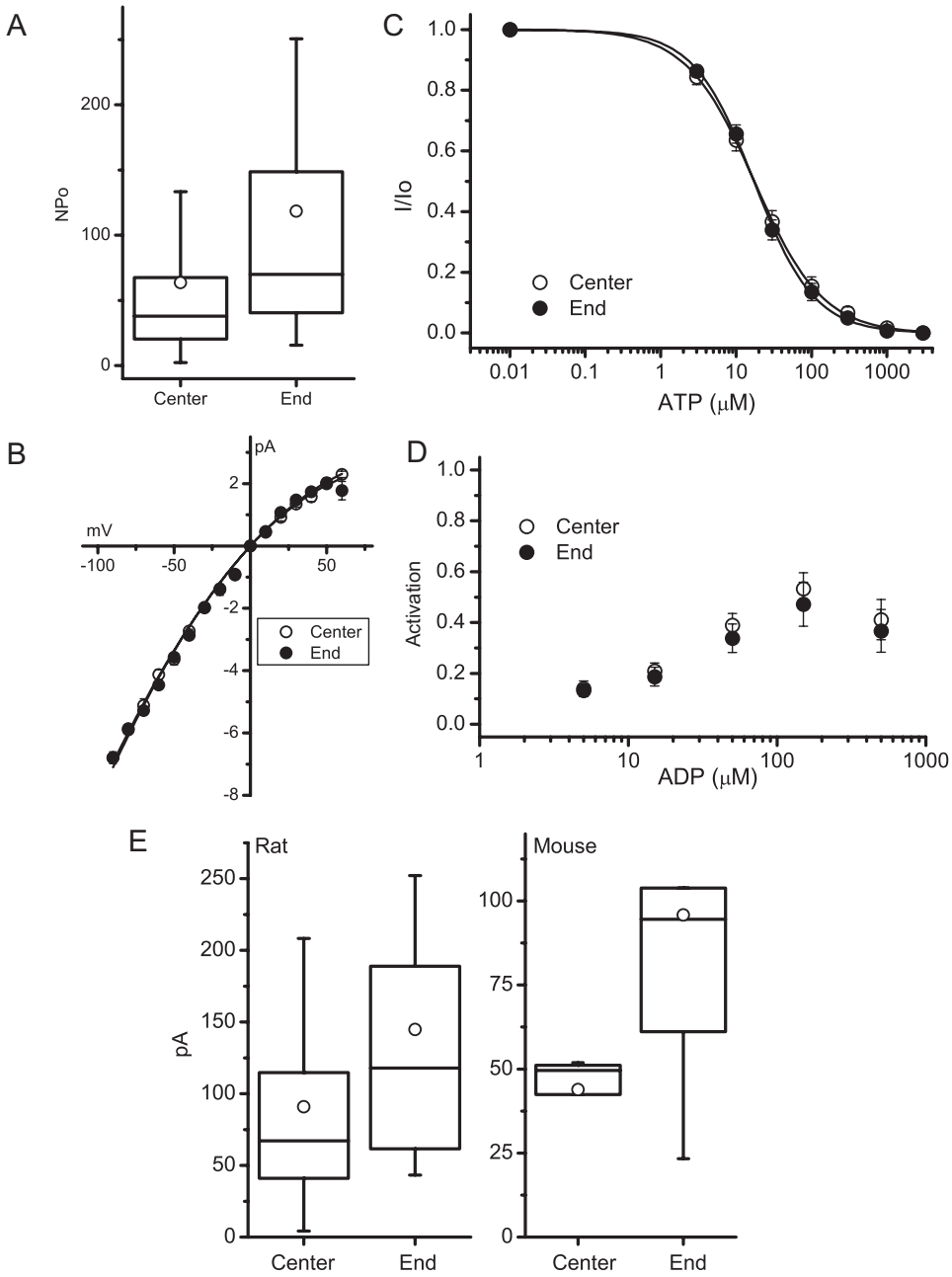

FIGURE 6. **Properties of local K_{ATP} channels recorded at the ICD and at the cell center.** Patches were obtained from the cell center or as close as feasible to the ICD end of the cell. Recordings were made in the inside-out configuration (*A–D*) or in cell-attached patch configuration (*E*). *A*, recordings of N.Po, (the number of channels multiplied by the apparent open probability) made immediately after patch excision to avoid rundown in the absence of ATP are shown as a box and whiskers plot. *B*, the K_{ATP} channel unitary current, recorded between −100 and +60 mV, are plotted as a function of the membrane potential. *C*, current (normalized to the maximal channel current in the absence of ATP; I_o) is plotted as a function of the ATP concentration. Shown are the means ± S.E. of cumulative data. The *solid lines* were produced by fitting the cumulative data points to a pseudo-Hill function (see "Experimental Procedures"), where I_o is the current in the absence of ATP, IC_{50} is the ATP concentration at which half-maximal inhibition occurs, and *h* is the Hill coefficient. The IC_{50} values were respectively 17.5 and 17.3 μM ATP for the cell center and cell end (the corresponding Hill coefficients were 0.96 and 1.1). *D*, activation of K_{ATP} channels by MgADP. Recordings of the mean patch current (*I*) were made in the presence of an ATP concentration close to half-maximal inhibition ($I_{1/2}$; 50 μM). The degree of activation by MgADP was normalized as $(I\,I_{1/2})/(I_o - I_{1/2})$. *E*, local K_{ATP} channel currents recorded in the cell-attached patch clamp configuration at the cell end or center. Membrane currents were recorded using a ramp voltage protocol (between −120 and 0 mV) before and after application of dinitrophenol (100 μM) to stimulate K_{ATP} channel opening. The DNP-activated current was variable, suggestive of K_{ATP} channel clustering. There was a trend for larger K_{ATP} channel currents to be recorded near the cell ends. We repeated this study using mouse ventricular myocytes, and although the difference appeared more pronounced, statistical significance was not achieved ($p = 0.058$; Student's *t* test).

lished biochemical studies (19). The IHC assay does not lend itself to examine how PKP2 deficiency influences endocytic recycling of K_{ATP} channels and/or their redistribution within subcellular compartments, which may further impact their surface density. This will be addressed in future biochemical experiments.

DISCUSSION

Our data demonstrate that K_{ATP} channel expression is concentrated at the ICD regions of ventricular myocytes, where they co-localize with desmosomal proteins (*e.g.*, PG and PKP2). Physical interaction of K_{ATP} channel subunits with these pro-

TABLE 1
K_{ATP} channel properties

	Wild type		PKP2 (+/−)	
	Center	End	Center	End
Unitary conductance (pS)	77 ± 2.6 (n = 5)	75 ± 1.4 (n = 10)	79 ± 1.0 (n = 8)	80 ± 1.0 (n = 7)
Mean patch current (pA)	414 ± 67.8 (n = 68)	769 ± 108.4 (n = 63)[a]	552 ± 60.9 (n = 49)	515 ± 50.9 (n = 50)
IC_{50}				
Value	28 ± 7.7 (n = 31)	18 ± 2.1 (n = 31)	19 ± 12.1 (n = 19)	30 ± 5.0 (n = 21)[a]
Median	14.5	13.2	14.0	22.8
Hill coefficient				
Value	1.2 ± 0.05 (n = 31)	1.3 ± 0.05 (n = 31)	1.3 ± 0.09 (n = 19)	1.2 ± 0.05 (n = 21)
Median	1.2	1.3	1.19	1.2

[a] $p < 0.05$ end *versus* center, analysis of variance on Ranks.

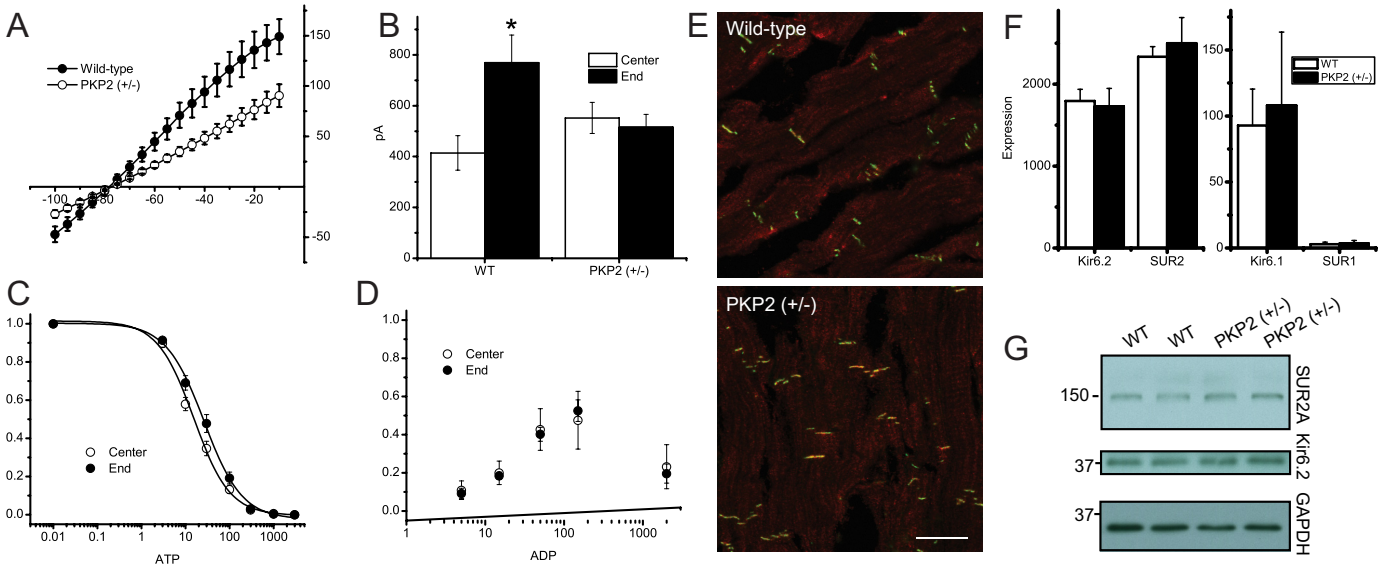

FIGURE 7. **K_{ATP} channel properties in cardiac myocytes from PKP2 (+/−) deficient mice.** *A*, whole cell current was recorded with ramp voltage pulses in cardiac myocytes before and after metabolic poisoning with DNP (100 μM). The DNP-activated current density (corrected for cell capacitance) is plotted as a function of membrane potential. *B*, mean patch current in the absence of ATP was recorded using the inside-out patch clamp configuration with patches obtained from the cell center or as close as possible to the ICD end of the cell. The data are plotted for wild-type or PKP2 (+/−) mice. *C*, ATP sensitivity of K_{ATP} channels from center or cell end of PKP2 (+/−) cardiac myocytes. *D*, degree of ADP stimulation of K_{ATP} channels from center or cell end of PKP2 (+/−) cardiac myocytes. *E*, immunohistochemistry performed using an anti-Kir6.2 antibody (Lee62; 1:200; *red*) and an antibody against N-cadherin (*green*). The *scale bar* represents 25 μm. *F*, mRNA expression of Kir6.2 and SUR2, relative to that of reference genes (RPS56 and HMBS), is shown for PKP2 and WT mouse heart. *G*, Western blotting of WT and PKP2 (+/−) mouse heart membranes with antibodies against SUR2A (M19; 1:300), Kir6.2 (C62, 1:2000), and GAPDH (1:8000).

teins was also demonstrated with co-immunoprecipitation experiments. The local K_{ATP} channel current density is higher when recorded at the intercalated disk ends of isolated cardiac myocytes compared with the cell center, but other properties (unitary conductance and nucleotide sensitivities) are similar. The whole cell K_{ATP} channel current density is reduced in myocytes isolated from PKP2 (+/−) mouse hearts, and the K_{ATP} channel current heterogeneity is reduced. Immunohistochemistry experiments reveal that K_{ATP} channels also co-localize with other ICD proteins, such as N-cadherin, AnkG, and DP and to a lesser extent with the gap junction protein Cx43.

Subcellular Localization of K_{ATP} Channels—The subcellular localization of many ion channels, exchangers, and pumps is nonuniform across a cardiac myocyte. One of the best characterized cases for polarized expression of a channel within cardiac myocytes is the preferential localization of Cx43 to the ICD (25). Other ion channels demonstrating spatial heterogeneity within cardiac myocytes include the K^+ channels Kv1.5 and Kir2.1 (3), as well as the Na^+ channel (4). The subcellular distribution and membrane anchoring of cardiac K_{ATP} channels are incompletely described. Early surface topology studies obtained with scanning ion conductance microscopy suggested a higher density of K_{ATP} channels within t-tubular openings (26), consistent with punctuate striated staining previously observed in immunohistochemistry experiments (15) (see also the immunohistochemistry data in the current study). Using different antibodies and optimized antibody concentrations, we have now identified K_{ATP} channel subunits also to be expressed at the intercalated disk regions of ventricular myocytes. We observed similar localization patterns when using a variety of antibodies against either Kir6.2 or SUR2A, which argues for specific staining by these antibodies. Staining was absent in cryosections of Kir6.2 knock-out mice (not shown), which further supports the concept that these antibodies detected the presence of K_{ATP} channel subunits in the cardiac intercalated disk regions, in addition to their well described localization in the sarcolemma of cardiac myocytes.

Properties of K_{ATP} Channels at the Intercalated Disk—We used patch clamp techniques to isolate patches near the center of cardiac myocytes or as close as possible toward the cell ends. The patch pipette resistance was monitored to ensure that the patch membrane surface area was comparable between cells.

However, because the patch electrode is lowered unto the top of the cell, this approach has the disadvantage that we are not directly examining channel properties at the vertical face of the cell junction. Furthermore, although we used high magnification objectives (40×), the optical resolution of the microscope is insufficient to ensure that the patch pipette is always placed in comparable locations. This may in part account for the variability that we observed in the local current densities. An alternative, but not mutually exclusive, explanation is that K_{ATP} channels are clustered on the cell surface. This possibility is supported by our super-resolution (dSTORM) images. Despite these limitations, we found that the local K_{ATP} channel current (median K_{ATP} channel patch current in the absence of ATP) was almost 2-fold higher at the cell ends compared with the cell center. Other properties of the K_{ATP} channels at the intercalated disk region were similar, including their unitary conductance, inhibition by ATP, and stimulation by MgADP. These data argue for the possibility that the intercalated disk K_{ATP} channels have a molecular composition that is not unlike that of the channels at the center of the myocyte. The larger K_{ATP} channel current density at the cell end is likely due, therefore, to elevated expression levels in this region of the cardiac myocyte.

Are There Two Distinct Populations of K_{ATP} Channels?—Data from the Mohler laboratory demonstrated that Kir6.2 physically interacts with ankyrin B and that K_{ATP} channel function is negatively affected in cardiac myocytes isolated from mice lacking ankyrin B (27). Ankyrin B mostly localizes to the lateral sides and t-tubules of cardiac myocytes and is expected to anchor K_{ATP} channels within these subcellular domains. These K_{ATP} channels may also interact with the dystrophin complex (28). This is a situation reminiscent of the population of lateral cardiac Na^+ channels, which interacts with the syntrophin-dystrophin complex (29). However, a second pool of cardiac Na^+ channels exists; these channels interact with SAP97 (29), AnkG (30), and PKP2 (31), and they are located at the ICD of cardiomyocytes (4). Polarized distribution of proteins within a cell is accomplished by directed delivery mechanisms and/or their stabilization on the cell surface. The latter can occur by binding to specific scaffolds, such as AnkG, which localizes predominantly to the ICD (30) and is responsible for targeting of Nav1.5 to this region (32). Moreover, recent data demonstrate that AnkG is a key functional component of the ICD and integrates the functionality at two cardiac junctional structures: gap junctions and the desmosome (32). We observed a high degree of co-localization of K_{ATP} channels with AnkG and postulate that AnkG is a scaffold responsible for stabilization of a protein complex that includes K_{ATP} channel subunits and proteins of the desmosome. Although direct interaction between Kir6.2 and AnkG may not occur (33), indirect interactions, or interactions with SUR2A, cannot be excluded.

Subcellular Structures Enriched in K_{ATP} Channels—We cannot make definitive conclusions regarding the subcellular structures containing ICD K_{ATP} channels. We found a poor correlation between K_{ATP} channels and Cx43 localization, suggesting that K_{ATP} channels are not present in gap junctions. With confocal microscopy, we found a high degree of co-localization of K_{ATP} channels with PKP2, PG, DP, and N-cadherin, suggesting the possibility that K_{ATP} channels are present in structures enriched in these proteins. Desmosomes and adherens junctions are classically considered as separate intercellular adhesive junctions that anchor intermediate filaments and actin cytoskeleton, respectively, at the plasma membrane of adjoining cells. Desmosomes consist of three families of proteins, desmosomal cadherins (desmoglein and desmocollin), armadillo proteins (PG and PKP2), and plakins (DP and plectin). With adherens junctions, in contrast, the cytoplasmic tails of Ca^{2+}-dependent cadherins interact in a mutually exclusive manner with either β-catenin or PG, which in turn links to α-catenins and the actin cytoskeleton (34). Recent data demonstrate some desmosomal proteins to be also present in ultrastructurally defined fascia adherens junctions (35). In this mixed type junctional structure, termed a hybrid adhering junction or area composita, αT-catenin recruits desmosomal proteins to form a mixed type, reinforced junction at the ICD that is attached to both the intermediate filaments and the actin cytoskeleton (36). It is possible that K_{ATP} channels are located in the vicinity of such junctions. Indeed, our super-resolution microscopy experiments demonstrated that K_{ATP} channels localize within nanometer distances of PKP2. Similar future experiments will be conducted to examine the subcellular localization of K_{ATP} channels relative to that of PG, N-cadherin, and the catenins.

Functional Relevance of K_{ATP} Channels at the ICD?—We can only speculate as to the mechanisms by which K_{ATP} channels at the ICD may contribute to excitability under physiological conditions. Previous data demonstrated functional interaction between K_{ATP} channels and the Na^+/K^+ pump (37). Interestingly, we found both α and β subunits of the Na^+/K^+ ATPase to be present in K_{ATP} channel immunoprecipitates (14). It may be possible, therefore, that K_{ATP} channels may have a flux coupling role in the restricted intercellular space of the ICD. With Na^+/K^+ pump activation, ATP is consumed, and this may decrease local submembrane ATP levels in the immediate vicinity of an adjacent K_{ATP} channel. This, in turn, would activate the K_{ATP} channel. Outward K^+ movement through the channel restores the extracellular K^+ just depleted by the Na^+/K^+ pump. Under ischemic conditions, when K_{ATP} channels open uncontrollably, excessive K^+ efflux into the diffusion-limited ICD extracellular space may lead to excessive K^+ accumulation, membrane potential depolarization, and Na^+ channel inactivation. This scenario predicts a relationship between K_{ATP} channel activity and ischemia-induced conduction slowing, which has previously been noted experimentally (10).

Possible Role of K_{ATP} Channels in AC?—The end to end connections between cardiomyocytes (at the ICD), contains specific junctional complexes. Desmosomes and adherens junctions are best known for mediating mechanical coupling between cells, but growing evidence points to an integrated nature of junctional complexes and how aberrant cell-cell coupling is mediated through defects in junctional proteins. Mutations in desmosomal proteins are linked to AC, characterized by fibrofatty infiltration, sustained ventricular tachycardia, and sudden cardiac death (2). Although it may be difficult to visualize the functional relationship between these structural ele-

ments and electrical events (arrhythmias), the picture has been clarified with recent data. Some ion channels, including the Na^+ channel and K^+ channels (Kv1.5 and Kir2.1) are enriched at the ICD (3, 4). Moreover, interaction between desmosomal proteins and Na^+ channels occurs, and disruption of the desmosomal complex affects the function of these channels (6). Our data, demonstrating that K_{ATP} channels are down-regulated in PKP2 deficient mice, suggest that K_{ATP} channels may share these properties. Patients with AC suffer from ventricular tachycardia and sudden death, but it is unknown how these patients respond to cardiac ischemic insults. Mice deficient of αT-catenin have a much greater incidence of ventricular arrhythmias following acute myocardial ischemia (38). The ~40% decrease of whole cell K_{ATP} channel density that we observed in PKP2 (+/−) mice suggests that desmosomal disorders might be associated with a diminished protective role of K_{ATP} channels.

REFERENCES

1. Pieperhoff, S., and Franke, W. W. (2007) The area composita of adhering junctions connecting heart muscle cells of vertebrates. IV. Coalescence and amalgamation of desmosomal and adhaerens junction components: Late processes in mammalian heart development. *Eur. J. Cell Biol.* **86,** 377–391
2. Delmar, M., and McKenna, W. J. (2010) The cardiac desmosome and arrhythmogenic cardiomyopathies. From gene to disease. *Circ. Res.* **107,** 700–714
3. Cheng, L., Yung, A., Covarrubias, M., and Radice, G. L. (2011) Cortactin is required for N-cadherin regulation of Kv1.5 channel function. *J. Biol. Chem.* **286,** 20478–20489
4. Lin, X., Liu, N., Lu, J., Zhang, J., Anumonwo, J. M., Isom, L. L., Fishman, G. I., and Delmar, M. (2011) Subcellular heterogeneity of sodium current properties in adult cardiac ventricular myocytes. *Heart Rhythm* **8,** 1923–1930
5. Milstein, M. L., Musa, H., Balbuena, D. P., Anumonwo, J. M., Auerbach, D. S., Furspan, P. B., Hou, L., Hu, B., Schumacher, S. M., Vaidyanathan, R., Martens, J. R., and Jalife, J. (2012) Dynamic reciprocity of sodium and potassium channel expression in a macromolecular complex controls cardiac excitability and arrhythmia. *Proc. Natl. Acad. Sci. U.S.A.* **109,** E2134–E2143
6. Cerrone, M., Noorman, M., Lin, X., Chkourko, H., Liang, F. X., van der Nagel, R., Hund, T., Birchmeier, W., Mohler, P., van Veen, T. A., van Rijen, H. V., and Delmar, M. (2012) Sodium current deficit and arrhythmogenesis in a murine model of plakophilin-2 haploinsufficiency. *Cardiovasc. Res.* **95,** 460–468
7. Rizzo, S., Lodder, E. M., Verkerk, A. O., Wolswinkel, R., Beekman, L., Pilichou, K., Basso, C., Remme, C. A., Thiene, G., and Bezzina, C. R. (2012) Intercalated disc abnormalities, reduced Na^+ current density, and conduction slowing in desmoglein-2 mutant mice prior to cardiomyopathic changes. *Cardiovasc. Res.* **95,** 409–418
8. Nichols, C. G. (2006) K_{ATP} channels as molecular sensors of cellular metabolism. *Nature* **440,** 470–476
9. Flagg, T. P., Kurata, H. T., Masia, R., Caputa, G., Magnuson, M. A., Lefer, D. J., Coetzee, W. A., and Nichols, C. G. (2008) Differential structure of atrial and ventricular K_{ATP}. Atrial K_{ATP} channels require SUR1. *Circ. Res.* **103,** 1458–1465
10. Bao, L., Kefaloyianni, E., Lader, J., Hong, M., Morley, G., Fishman, G. I., Sobie, E. A., and Coetzee, W. A. (2011) Unique properties of the ATP-sensitive K^+ channel in the mouse ventricular cardiac conduction system. *Circ. Arrhythm. Electrophysiol.* **4,** 926–935
11. Zingman, L. V., Zhu, Z., Sierra, A., Stepniak, E., Burnett, C. M., Maksymov, G., Anderson, M. E., Coetzee, W. A., and Hodgson-Zingman, D. M. (2011) Exercise-induced expression of cardiac ATP-sensitive potassium channels promotes action potential shortening and energy conservation. *J. Mol. Cell Cardiol.* **51,** 72–81
12. Zingman, L. V., Hodgson, D. M., Bast, P. H., Kane, G. C., Perez-Terzic, C., Gumina, R. J., Pucar, D., Bienengraeber, M., Dzeja, P. P., Miki, T., Seino, S., Alekseev, A. E., and Terzic, A. (2002) Kir6.2 is required for adaptation to stress. *Proc. Natl. Acad. Sci. U.S.A.* **99,** 13278–13283
13. Tong, X., Porter, L. M., Liu, G., Dhar-Chowdhury, P., Srivastava, S., Pountney, D. J., Yoshida, H., Artman, M., Fishman, G. I., Yu, C., Iyer, R., Morley, G. E., Gutstein, D. E., and Coetzee, W. A. (2006) Consequences of cardiac myocyte-specific ablation of K_{ATP} channels in transgenic mice expressing dominant negative Kir6 subunits. *Am. J. Physiol. Heart Circ. Physiol.* **291,** H543–H551
14. Hong, M., Kefaloyianni, E., Bao, L., Malester, B., Delaroche, D., Neubert, T. A., and Coetzee, W. A. (2011) Cardiac ATP-sensitive K^+ channel associates with the glycolytic enzyme complex. *FASEB J.* **25,** 2456–2467
15. Morrissey, A., Rosner, E., Lanning, J., Parachuru, L., Dhar Chowdhury, P., Han, S., Lopez, G., Tong, X., Yoshida, H., Nakamura, T. Y., Artman, M., Giblin, J. P., Tinker, A., and Coetzee, W. A. (2005) Immunolocalization of K_{ATP} channel subunits in mouse and rat cardiac myocytes and the coronary vasculature. *BMC Physiol.* **5,** 1
16. Bolte, S., and Cordelières, F. P. (2006) A guided tour into subcellular colocalization analysis in light microscopy. *J. Microsc.* **224,** 213–232
17. van de Linde, S., Löschberger, A., Klein, T., Heidbreder, M., Wolter, S., Heilemann, M., and Sauer, M. (2011) Direct stochastic optical reconstruction microscopy with standard fluorescent probes. *Nat. Protoc.* **6,** 991–1009
18. Henriques, R., Lelek, M., Fornasiero, E. F., Valtorta, F., Zimmer, C., and Mhlanga, M. M. (2010) QuickPALM. 3D real-time photoactivation nanoscopy image processing in ImageJ. *Nat. Methods* **7,** 339–340
19. Bao, L., Hadjiolova, K., Coetzee, W. A., and Rindler, M. J. (2011) Endosomal K_{ATP} channels as a reservoir after myocardial ischemia. A role for SUR2 subunits. *Am. J. Physiol. Heart Circ. Physiol.* **300,** H262–H270
20. Dhar-Chowdhury, P., Harrell, M. D., Han, S. Y., Jankowska, D., Parachuru, L., Morrissey, A., Srivastava, S., Liu, W., Malester, B., Yoshida, H., and Coetzee, W. A. (2005) The glycolytic enzymes, glyceraldehyde-3-phosphate dehydrogenase, triose-phosphate isomerase, and pyruvate kinase are components of the K_{ATP} channel macromolecular complex and regulate its function. *J. Biol. Chem.* **280,** 38464–38470
21. Malkusch, S., Endesfelder, U., Mondry, J., Gelléri, M., Verveer, P. J., and Heilemann, M. (2012) Coordinate-based colocalization analysis of single-molecule localization microscopy data. *Histochem. Cell Biol.* **137,** 1–10
22. Heilemann, M., van de Linde, S., Schüttpelz, M., Kasper, R., Seefeldt, B., Mukherjee, A., Tinnefeld, P., and Sauer, M. (2008) Subdiffraction-resolution fluorescence imaging with conventional fluorescent probes. *Angew. Chem. Int. Ed. Engl.* **47,** 6172–6176
23. Mohler, P. J., Rivolta, I., Napolitano, C., LeMaillet, G., Lambert, S., Priori, S. G., and Bennett, V. (2004) Nav1.5 E1053K mutation causing Brugada syndrome blocks binding to ankyrin-G and expression of Nav1.5 on the surface of cardiomyocytes. *Proc. Natl. Acad. Sci. U.S.A.* **101,** 17533–17538
24. Grossmann, K. S., Grund, C., Huelsken, J., Behrend, M., Erdmann, B., Franke, W. W., and Birchmeier, W. (2004) Requirement of plakophilin 2 for heart morphogenesis and cardiac junction formation. *J. Cell Biol.* **167,** 149–160
25. Delmar, M. (2004) The intercalated disk as a single functional unit. *Heart Rhythm.* **1,** 12–13
26. Korchev, Y. E., Negulyaev, Y. A., Edwards, C. R., Vodyanoy, I., and Lab, M. J. (2000) Functional localization of single active ion channels on the surface of a living cell. *Nat. Cell Biol.* **2,** 616–619
27. Li, J., Kline, C. F., Hund, T. J., Anderson, M. E., and Mohler, P. J. (2010) Ankyrin-B regulates Kir6.2 membrane expression and function in heart. *J. Biol. Chem.* **285,** 28723–28730
28. Graciotti, L., Becker, J., Granata, A. L., Procopio, A. D., Tessarollo, L., and Fulgenzi, G. (2011) Dystrophin is required for the normal function of the cardio-protective K_{ATP} channel in cardiomyocytes. *PLoS One* **6,** e27034
29. Petitprez, S., Zmoos, A. F., Ogrodnik, J., Balse, E., Raad, N., El-Haou, S., Albesa, M., Bittihn, P., Luther, S., Lehnart, S. E., Hatem, S. N., Coulombe, A., and Abriel, H. (2011) SAP97 and dystrophin macromolecular complexes determine two pools of cardiac sodium channels Nav1.5 in cardiomyocytes. *Circ. Res.* **108,** 294–304
30. Lowe, J. S., Palygin, O., Bhasin, N., Hund, T. J., Boyden, P. A., Shibata, E.,

Anderson, M. E., and Mohler, P. J. (2008) Voltage-gated Nav channel targeting in the heart requires an ankyrin-G dependent cellular pathway. *J. Cell Biol.* **180,** 173–186
31. Sato, P. Y., Musa, H., Coombs, W., Guerrero-Serna, G., Patiño, G. A., Taffet, S. M., Isom, L. L., and Delmar, M. (2009) Loss of plakophilin-2 expression leads to decreased sodium current and slower conduction velocity in cultured cardiac myocytes. *Circ. Res.* **105,** 523–526
32. Sato, P. Y., Coombs, W., Lin, X., Nekrasova, O., Green, K. J., Isom, L. L., Taffet, S. M., and Delmar, M. (2011) Interactions between ankyrin-G, Plakophilin-2, and Connexin43 at the cardiac intercalated disc. *Circ. Res.* **109,** 193–201
33. Kline, C. F., Kurata, H. T., Hund, T. J., Cunha, S. R., Koval, O. M., Wright, P. J., Christensen, M., Anderson, M. E., Nichols, C. G., and Mohler, P. J. (2009) Dual role of K_{ATP} channel C-terminal motif in membrane targeting and metabolic regulation. *Proc. Natl. Acad. Sci. U.S.A.* **106,** 16669–16674
34. Rudini, N., and Dejana, E. (2008) Adherens junctions. *Curr. Biol.* **18,** R1080–R1082
35. Franke, W. W., Borrmann, C. M., Grund, C., and Pieperhoff, S. (2006) The area composita of adhering junctions connecting heart muscle cells of vertebrates. I. Molecular definition in intercalated disks of cardiomyocytes by immunoelectron microscopy of desmosomal proteins. *Eur. J. Cell Biol.* **85,** 69–82
36. Li, J., and Radice, G. L. (2010) A new perspective on intercalated disc organization. Implications for heart disease. *Dermatol. Res. Pract.* **2010,** 207835
37. Priebe, L., Friedrich, M., and Benndorf, K. (1996) Functional interaction between K_{ATP} channels and the Na^+-K^+ pump in metabolically inhibited heart cells of the guinea-pig. *J. Physiol.* **492,** 405–417
38. Li, J., Goossens, S., van Hengel, J., Gao, E., Cheng, L., Tyberghein, K., Shang, X., De Rycke, R., van Roy, F., and Radice, G. L. (2012) Loss of αT-catenin alters the hybrid adhering junctions in the heart and leads to dilated cardiomyopathy and ventricular arrhythmia following acute ischemia. *J. Cell Sci.* **125,** 1058–1067